Unveiling Unexpected Modulator-CO_2 Dynamics Within a Zirconium Metal-Organic Framework

Thomas M. Rayder,[1] Filip Formalik,[2,3] Simon M. Vornholt,[4] Hilliary Frank,[5] Seryeong Lee,[1] Maytham Alzayer,[2] Zhihengyu Chen,[4] Debabrata Sengupta,[1] Timur Islamoglu,[1] Francesco Paesani,[5] Karena W. Chapman,[4] Randall Q. Snurr,[2] and Omar K. Farha[1,*]

[1]Department of Chemistry, Northwestern University, Evanston, IL 60208

[2]Department of Chemical & Biological Engineering, Northwestern University, Evanston, IL 60208, United States

[3]Department of Micro, Nano, and Bioprocess Engineering, Faculty of Chemistry, Wroclaw University of Science and Technology, 50-370 Wroclaw, Poland

[4]Department of Chemistry, Stony Brook University, Stony Brook, NY 11794

[5]Department of Chemistry and Biochemistry, University of California, San Diego, La Jolla, CA 92037

ABSTRACT: Carbon capture, storage, and utilization (CCSU) represents an opportunity to mitigate carbon emissions that drive global anthropogenic climate change. Promising materials for CCSU through gas adsorption have been developed by leveraging the porosity, stability, and tunability of extended crystalline coordination polymers called metal-organic frameworks (MOFs). While the development of these frameworks has yielded highly effective CO_2 sorbents, an in-depth understanding of the properties of MOF pores that lead to the most efficient uptake during sorption would benefit the rational design of more efficient CCSU materials. Though previous investigations of gas-pore interactions often assumed that the internal pore environment was static, discovery of more dynamic behavior represents an opportunity for precise sorbent engineering. Herein, we report a multifaceted *in situ* analysis following the adsorption of CO_2 in MOF-808 variants with different capping agents (formate, acetate, and trifluoroacetate – FA, AA, and TFA, respectively). *In situ* diffuse reflectance infrared Fourier transform spectroscopy (DRIFTS) analysis paired with multivariate analysis tools and *in situ* powder X-ray diffraction revealed unexpected CO_2 interactions at the node associated with dynamic behavior of node-capping modulators in the pores of MOF-808, which had previously been assumed to be static. MOF-808-TFA displays two binding modes, resulting in higher binding affinity for CO_2. Computational analyses further support these dynamic observations. The beneficial role of these structural dynamics could play an essential role in building a deeper understanding of CO_2 binding in MOFs.

Introduction

The rapid rise in atmospheric CO_2 concentration and consequent warming climate have resulted in an increased frequency of disastrous weather events and irreversible damage to various ecosystems, posing a significant concern to societal wellbeing.[1] Removal of greenhouse gases from the atmosphere or preemptive capture of industrially produced gases could potentially mitigate these effects.[2–4] Significant recent effort has focused on achieving this goal by developing and discovering new materials with high affinity and selectivity for CO_2.[5] These materials are often porous and crystalline, affording high internal surface area and recyclability. Materials such as zeolites and porous silica have been well-studied for such applications,[6,7] owing in part to their production on an industrial scale. While these materials are effective and reusable sorbents, they can exhibit variance in bulk structure, complicating detailed mechanistic investigations, or suffer from low selectivity for CO_2 in the presence of water vapor.[7,8]

Metal-organic frameworks (MOFs) are a tunable alternative to these sorbents that have molecularly defined structures paired with high porosity.[9–11] These coordination polymers are composed of metal ion or metal cluster nodes and organic bridging linkers that self-assemble into extended crystals.[12,13] An extensive library of MOFs has been developed from a variety of components,[14] some of which exhibit superior CO_2 sorption. While many of these sorbents depend on physisorptive interactions between the gas and the internal MOF pores,[15,16] the introduction of platforms for chemisorption in MOFs has led to significant improvement in gas uptake, especially at low partial pressures.[17–19] Detailed understanding of the mechanism that is operative during such strong interactions can inform further logical design and development of new CO_2 sorption materials.

Zirconium-based MOFs[20,21] are well-regarded for their stability[22,23] and ease of synthesis,[20] as well as their catalytic properties[24–26] and tunability,[27–31] and have been successfully employed for gas sorption.[32] The most widely studied of these MOFs, are UiO-66,[33] NU-1000,[34] and MOF-808[35] all composed of zirconium-oxo cluster nodes with 12 potential linker binding sites. The Zr-nodes of these MOFs are 12-connected, 8-connected, and 6-connected, respectively, with the sites that are not bound to linkers usually capped by the

modulators used during synthesis or other coordinating groups present in solution such as hydroxide. Removal of the capping modulators from these sites uncovers Lewis acidic zirconium sites, which can be leveraged for binding of targeted guests,[24] catalysis,[29,36,37] and ligand substitution reactions to further tune the properties of the MOF.[30,38,39] Importantly, UiO-66, NU-1000, and MOF-808 are all composed of symmetric unit cells, circumventing analytical complications associated with similar but asymmetric 9-connected MOFs.[40,41] The pore geometry of 3,6-connected MOF-808, which contains large adamantane-shaped cages (18.4 Å) and smaller tetrahedral cages (10 Å), minimizes steric inhibition about the node and allows for easier access to open zirconium sites than its more connected counterparts.

We have previously investigated the effect of the node-capping modulator in MOF-808 on water sorption and the detoxification of chemical warfare agents,[42] observing significant variance in MOF behavior depending on which modulator was used during synthesis. While the influence of capping group identity on CO_2 sorption in MOF-808 has been probed using postsynthetic substitution reactions,[43–45] we are not aware of any studies varying the modulator during synthesis for the purpose of investigating CO_2 adsorption mechanisms. Further, MOF-808 has been synthesized using a variety of modulators, making it a promising platform for studying these effects. Additionally, while previous studies assumed that the capping carboxylate groups were static and inhibited direct chemisorption of gases to open metal sites, recent reports have explored the dynamic nature of the bonds between nodes and bridging carboxylate linkers.[29,36,39,46–48] Ostensibly, carboxylate modulators could be similarly labile, exposing open metal sites for direct sorption. Such lability might manifest in the form of shifting sorption behavior with increasing electron withdrawing characteristic of the capping modulator, which should decrease the strength of the Zr-$O_{modulator}$ bonds in the framework (Scheme 1). Described herein is a mechanistic investigation of CO_2 sorption in MOF-808-X (X = capping modulator) and the dynamic role that the node-capping modulator plays, insights from which can lead to the enhancement and improvement of other CO_2 adsorption materials.

Scheme 1. CO_2 sorption behavior changes with increasingly electron-withdrawing node-capping modulator in MOF-808

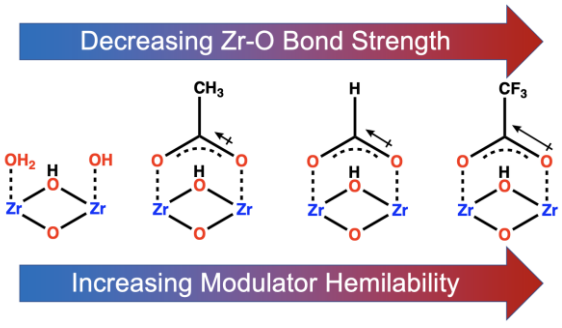

Results and Discussion

While previous reports have investigated the influence of various MOF characteristics on adsorbent properties, few have isolated the effect of the modulator used during synthesis, which can lead to notable differences in structure and behavior. To selectively probe these effects for MOF-808 and avoid batch-to-batch variation, several variants of MOF-808-X synthesized using formic acid, acetic acid, or trifluoroacetic acid as a modulator (X = FA, AA, and TFA, respectively) were prepared using previously established protocols for large-batch aqueous synthesis and characterized by NMR spectroscopy (Fig, S1-S3) to quantify the number of capping modulators per MOF node.[42] MOF-808-OH, in which the modulator is removed and the resulting zirconium nodes are capped by one hydroxyl and one aquo ligand per modulator site, was prepared by treatment of MOF-808-FA with hydrochloric acid and characterized by digested NMR to confirm successful removal of the modulator (Figure S4).[49,50] Powder X-ray diffraction, N_2 sorption, and SEM analyses indicated that each variant was crystalline, porous, and exhibited similar morphology (Figures S5-S14), meaning that variance in these characteristics would not be the root cause of differences in other behavior.

Figure 1. CO_2 adsorption isotherms in MOF-808-X at

While the only variance in the N_2 sorption capacity of MOF-808-X variants as a function of modulator identity was lower adsorption capacity in MOF-808-TFA due to decreased average pore size (Figure S15), notable variation following a different trend was observed for CO_2 sorption at 298.15 K (Figure 1). MOF-808-TFA exhibited the highest capacity, while little difference was observed between MOF-808-FA and MOF-808-AA, and MOF-808-OH was significantly less effective for adsorbing CO_2 than modulator-capped analogs. Similar trends held for isotherms collected at 273.15 K, 288.15 K, and 313.15 K (Figures S16-18), consistent with these variations in sorption being a consequence of structural differences among the MOFs. The observed trend in CO_2 adsorption was different from that observed for N_2 at high loadings (Figure S6 and S7) but was similar to that at very low partial pressures (Figure S15). This dichotomy suggests that decreased size in the adamantane-shaped pores in MOF-808-TFA promoted adsorption at low loadings but limited it at higher loadings while the larger pores of other variants led to improved adsorption at higher pressures. It was also apparent that access to the smaller, tetrahedral MOF pores was not the cause, as MOF-808-OH should exhibit the highest capacity in that case owing to the increased steric accessibility to these cages in the absence of modulator.

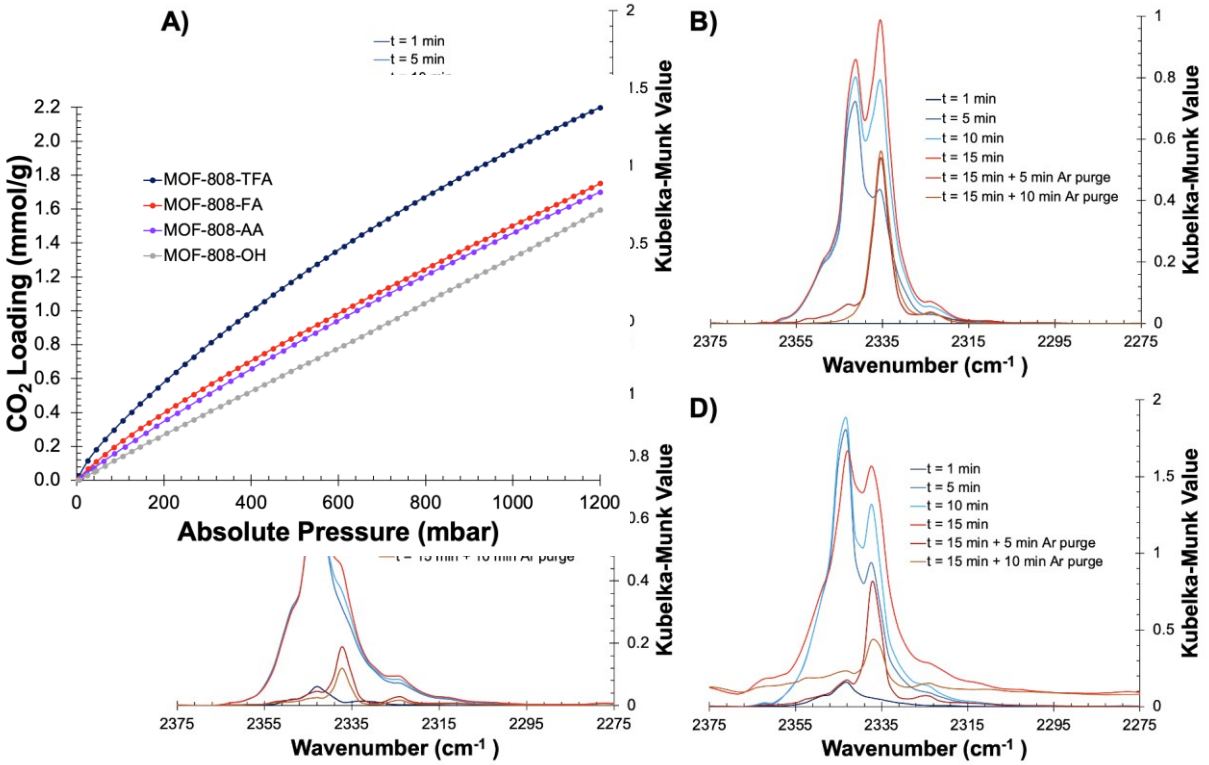

Figure 2. DRIFTS difference spectra in the region associated with CO_2 adsorption asymmetric stretching mode for MOF-808-X where X = A) TFA, B) FA, C) AA, and D) OH, collected under a flow of 5% CO_2 (balance Ar) at 30 ºC at various time points

In the interest of developing a further understanding of this behavior, we next calculated the heat of adsorption (Q_{ST}) for CO_2 in each variant based on these isotherms (Figure S19). While little difference was observed among variants at especially low coverage, more distinct gaps could be observed above 5 cm^3/g. Although differences among variants were negligible for the most part, MOF-808-TFA exhibited the highest Q_{ST} (~26 kJ/mol) at these higher loadings, while MOF-808-AA and -FA behaved almost identically (~24 kJ/mol). The lowest Q_{ST} (~20 kJ/mol) was observed for MOF-808-OH, consistent with the CO_2 physisorption capacity among variants.

To obtain more precise mechanistic insight into adsorption behavior in MOF-808-X, *in situ* DRIFTS difference spectra of each variant were obtained at several time points leading up to 15 minutes under a flow of 5% CO_2 and 95% argon at 298.15 K. While the expected asymmetric stretching mode for CO_2 physisorption (2339-2343 cm^{-1}, bulk CO_2 = 2349 cm^{-1}) grew in intensity with time, another unexpected lower frequency stretch between 2333 and 2337 cm^{-1} appeared simultaneously (Figure 2).[51] Notably, while the higher-frequency peak disappeared when the sample was purged with argon at 298.15 K, this lower-frequency stretch remained. The intensity of the lower-frequency stretch was dependent on the identity of the modulator, with the highest intensity exhibited by MOF-808-TFA and the lowest by MOF-808-AA. This stretch was observed in MOF-808-OH as well, likely owing to a small amount of residual formate modulator in the framework after acid treatment. The intensity of this stretch did not correlate to the measured CO_2 adsorption capacity or previously calculated Qst values. This finding suggested that this stretch was a consequence of a process separate from physisorption, which dominates adsorption characteristics above the low CO_2 loadings tested in these DRIFTS experiments. Additionally, relatively little variance in the higher-frequency stretch among samples suggests that the stretch at ~2335 cm^{-1} is directly related to the presence and identity of the capping modulator, while the stretch at ~2339 cm^{-1} is not. Shifts in the frequency of typical stretches in the carboxylate region of the IR spectra (Figures S26-S30) indicated that the coordination of the capping modulator also changed during the process of CO_2 sorption in conjunction with the appearance of the lower-frequency peak, especially in MOF-808-TFA.

To further deconvolute the evolution of the observed DRIFTS stretches for MOF-808-X, these time-resolved data were processed using non-negative matrix factorization (NMF) (Figure 3).[52,53] NMF reduces complex data series to a smaller number of variables – i.e., a component and weighting matrix – which represent the contribution of component signals. Analysis by NMF indicates that two distinct DRIFTS signals evolve during CO_2 sorption: a higher frequency signal at 2343 cm^{-1} (component 1) and a lower frequency signal at 2335 cm^{-1} (component 2). These two components correspond well with the two stretches observed for MOF-808-TFA at 15 minutes, suggesting two separate modes of CO_2 sorption. The respective weighting matrices (Figure 3B) highlight the change in relative weights of components as CO_2 is dosed in and as the system is purged with argon. The observed matrix trends further clarify the spectroscopic behavior of MOF-808-X. MOF-808-TFA exhibits its two sorption regimes by DRIFTS, the first including growth of both signals in the presence of CO_2 in which both components increase in intensity and the second being

purging with argon, in which the intensity of component 1 is reduced while component 2 more effectively retains intensity. MOF-808-FA behaves similarly but exhibits much lower relative intensity for both components compared to the -TFA variant. As expected, MOF-808-OH exhibits the highest relative intensity for component 1 as well as contributions of component 2, directly linked to the remaining FA capping ligand after acid treatment. The intensity of component 2 is lowest in MOF-808-AA and sudden decay of component 1 is observed once the system is purged, which further supports the modulator dependency of adsorption behavior for CO_2 in MOF-808-X.

Such unexpected spectroscopic behavior continued at temperatures ranging from -60 ºC to 80 ºC (Figure 4 and Figures S31-S42). Additionally, the variance in intensity of each stretch provided further insight into the cause of the lower-frequency stretch. Consistent with physisorption behavior, the intensity of the high-frequency peak (Figure 4 and 5A) was highest at lower temperatures where the free energy of adsorption is dominated by the enthalpic contribution rather than the entropic component.

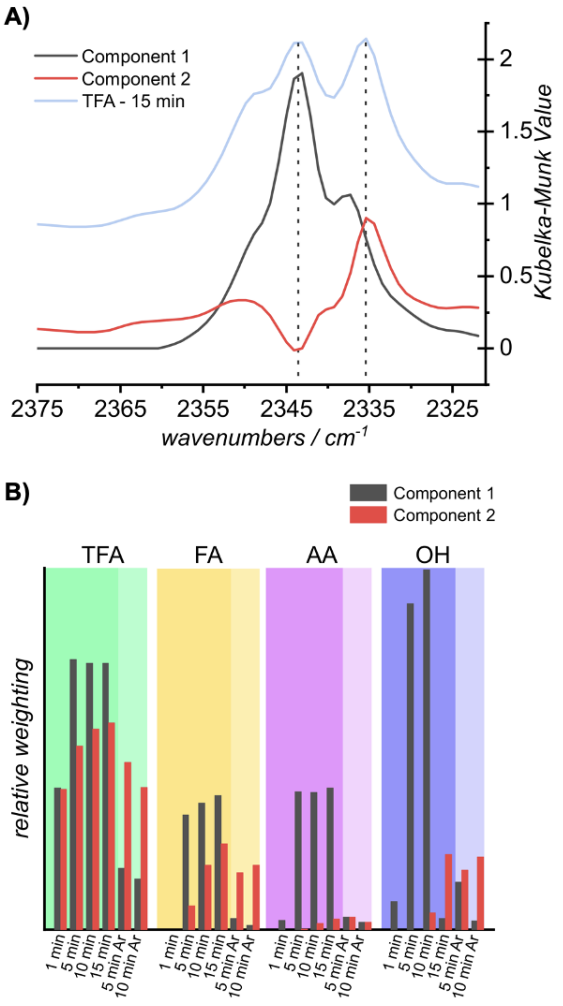

However, the lower-frequency stretch followed a different trend (Figure 5B). This stretch increased in intensity with increasing temperature for all samples containing node-capping modulators, reaching a maximum intensity at a different temperature depending on modulator identity (30 ºC for MOF-808-TFA and -FA, 60 ºC for MOF-808-AA), then decreased as expected with increasing temperature. Such initially counterintuitive behavior indicates that the

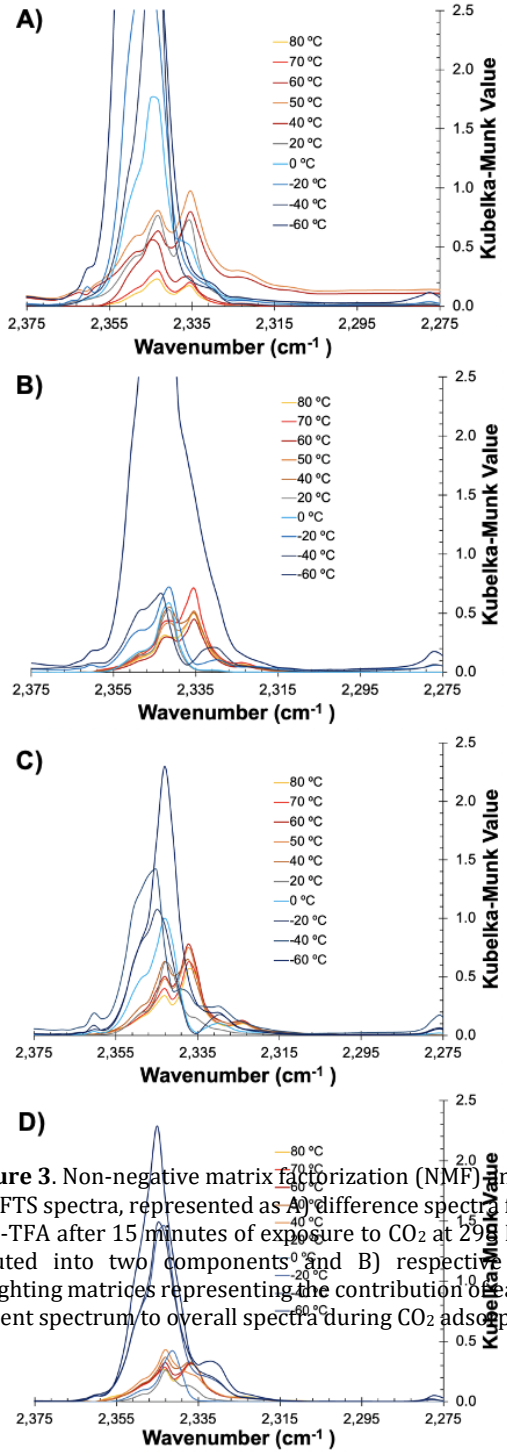

Figure 3. Non-negative matrix factorization (NMF) analysis of DRIFTS spectra, represented as A) difference spectra for MOF-808-TFA after 15 minutes of exposure to CO_2 at 298 K deconvoluted into two components and B) respective relative weighting matrices representing the contribution of each component spectrum to overall spectra during CO_2 adsorption and [illegible] difference spectra [illegible]orption asymmetric stretching mode for MOF-808-X where X = A) TFA, B) FA, C) AA, and D) OH, collected under a flow of 5% CO_2 (balance Ar) at 15 minutes at temperatures from -60 to 80 ºC.

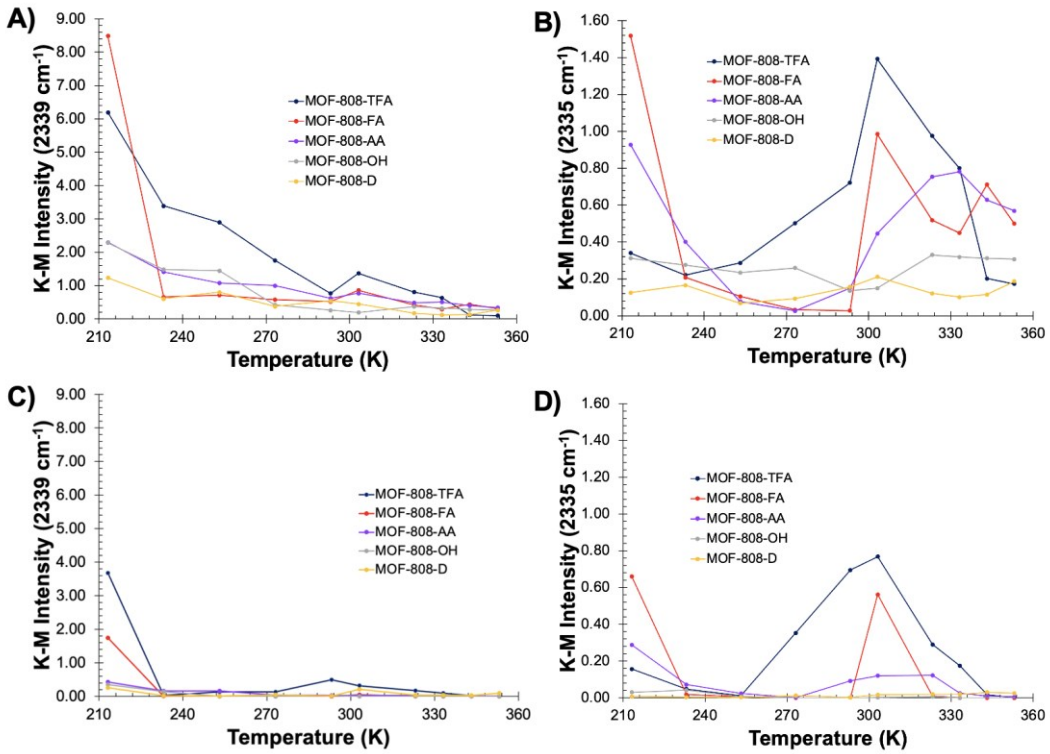

Figure 5. Trends observed in the intensity of variable temperature DRIFTS peaks for MOF-808-X under a flow of 5% CO_2 (balance Ar) at 15 minutes at A) 2339 cm^{-1} and B) 2335 cm^{-1}, and after 10 minutes purging with 100% Ar thereafter at C) 2339 cm^{-1}, and D) 2335 cm^{-1}

lower-frequency stretch results from a process for which a modulator-dependent activation energy must be overcome, suggesting a chemisorption pathway. The absence of such temperature dependence in the intensity of the lower-frequency peak for MOF-808-OH or its fully dehydrated analog MOF-808-D[54,55] further supports the hypothesis of modulator-dependent chemisorption, as access to the bare zirconium of the MOF node is most unimpeded in the absence of capping modulator. Similar temperature-dependent trends were observed when the samples were purged with argon for 10 minutes (Figure 5C and D). Very little signal was observed for either stretch in MOFs without capping modulator (MOF-808-OH and MOF-808-D) (Figures S38 and S40), suggesting full desorption of any adsorbed CO_2. Similarly, the high-frequency stretch was either absent or observed in very low intensity for samples with capping modulator above cryogenic temperatures after purging with argon. However, the low-frequency stretch intensity followed a similar trend to that during sorption for MOF-808-TFA, -AA, and –FA (Figure 5D), as intensity reached a maximum at elevated temperatures (40 ºC for MOF-808-TFA, and -FA, 50 ºC for MOF-808-AA). In conjunction, these data indicate that the high-frequency peak describes physisorption of CO_2 and the lower-frequency peak corresponds to a different process – likely chemisorption – that is both stronger than physisorption and involves the capping modulator. This is further supported by significant underprediction by GCMC calculated isotherms (Figure S46) indicating interactions going beyond physisorption.

MOF-808 is one of a family of zirconium-based MOFs in which the modulator caps open zirconium sites on the node. Two others are UiO-66, which exhibits no open metal sites in an ideal structure but often contains modulator-capped missing-linker defects, and NU-1000, a channel-type MOF in which four pairs of open metal sites per node are capped by modulators. Importantly, the linker geometry about the nodes of UiO-66 and NU-1000 leads to more steric crowding than in MOF-808. To determine whether this difference in geometry influences the behavior of CO_2 and whether the observed spectroscopic behavior was unique to MOF-808 or characteristic of zirconium MOFs in general, similar variable-temperature DRIFTS experiments were conducted with UiO-66 and NU-1000 (Figures S47 and S48). While a small signal at around 2335 cm^{-1} has previously been reported for UiO-66,[56] the sharp stretch observed for MOF-808 was absent for formate-capped variants of UiO-66 or NU-1000. The absence of this stretch suggests that the unique geometry of the 6-connected node in MOF-808 influences the behavior leading to the lower-frequency peak. One possible explanation for this is a more open pathway due to a less sterically crowded node allowing for dynamic modulator coordination and therefore enabling CO_2 to directly access the bare zirconium of the node.

Two potential operative pathways can thus be proposed for such direct adsorption of CO_2 to the MOF node: full dissociation of the modulator to leave two bare zirconium sites or hemilabile dissociation of one oxygen of the capping modulator from zirconium and coordination of this labile oxygen to a different atom nearby during sorption to uncover one zirconium site. To test the former, a sample of each variant was digested before and after *in situ* DRIFTS measurements, using NaOD in D_2O to determine whether the ratio of modulator to BTC linker had changed by ^{1}H NMR spectroscopy (Figures S1, S2, and S4) for MOF-808-FA, -AA, and -OH and by a combination ^{19}F NMR and ^{1}H NMR spectroscopy with an internal standard in NaOD/DMSO-d6 for

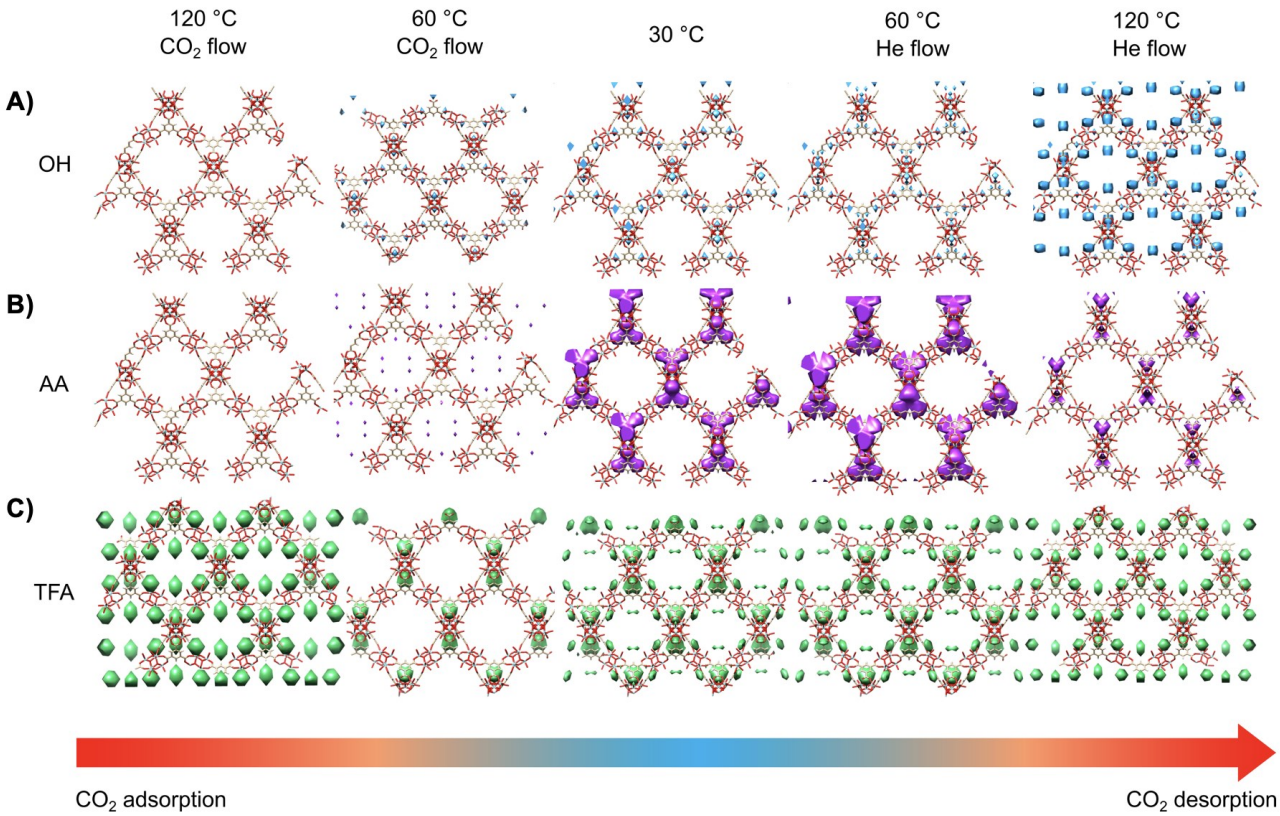

MOF-808-TFA (Figure S3). In all cases, the ratio of modulator to linker remained unchanged, suggesting that any modulator initially present in the MOF remained present after sorption and thus likely remained bound in some way to the node throughout the process.

In situ powder X-ray diffraction (PXRD) data were collected for MOF-808-TFA, -AA, and -OH upon adsorption and desorption of CO_2 in the temperature range 30-120 °C. The close correspondence of the PXRD data for the pristine and adsorption/temperature-cycled materials confirm their stability (Figure S49). Differential envelope densities (DEDs) were derived from the PXRD data to locate electron density associated with the CO_2 guest within the MOF pores (Figure 6). For MOF-808-AA and -OH, no guest electron density was observed following CO_2 exposure at 120 °C (Figure 6A and B). Upon cooling to 60 °C, electron density associated with adsorbed CO_2 was observed in the larger pore for -AA and in the smaller tetragonal pore for -OH, seemingly corresponding to the initial physisorption peak denoted by component 1 in the discussed NMF data (Figure 3). At 30 °C, the CO_2 was localized near the smaller tetragonal pore for both -AA and -OH. Progressive heating to 120 °C under helium to remove CO_2 reveals a hysteresis in adsorption. The DEDs indicate that the guests become more delocalized and are partially but not fully removed at 120 °C within the 1.5 minutes of the measurement. By contrast, MOF-808-TFA exhibits CO_2 adsorption even at 120 °C (Figure 6C). As with other variants, CO_2 adsorbs first near the smaller tetragonal pore at 60 °C, but then occupies a second binding site close to the Zr node at 30 °C. This indicates a secondary, potentially chemisorptive, adsorption site. This guest arrangement persists during subsequent heating to 60 °C and at 120 ºC as the timeframe of the measurement was insufficient to fully eliminate adsorbed CO_2 guests. The structural analysis of the *in situ* X-ray scattering during adsorption of CO_2 further supported direct adsorption of CO_2 to the zirconium node and suggested modulator hemilability, as capping modulator – especially in the presence of electron-rich fluorine of TFA – would repel the guest and result in greater density near the MOF linkers.

These findings were further supported by radial distribution function (RDF) data constructed from molecular dynamics (MD) simulations (Figure S50) run for 500 ps under thermal-isobaric conditions for MOF-808-FA. Such RDF plots describe the distance between the oxygens of CO_2 and the Zr atoms in the framework during these simulations. Across simulations, four predominant distance regions emerged, the smallest being between 2.8 – 3.0 Å, slightly longer than the Zr-O bonds of the framework. At the lowest pressures (Figure S50A), the distance between Zr and the CO_2 oxygen is most likely around 2.8 Å. As pressure increases and more CO_2 molecules enter the MOF framework, a more even distribution evolves, reflecting a shift to physisorption at other available sites (Fig S50B-F), consistent with the observed CO_2 isotherms.

Figure 6. Representations of differential envelope densities (DEDs) that reflect the locations of electron density from adsorbed CO_2 within MOF-808-X (X= A) -OH, B) -AA, C) -TFA). These were derived from *in situ* PXRD data collected during CO_2 adsorption upon cooling from 120 °C to 30 °C in a CO_2 atmosphere, and subsequent CO_2 desorption upon reheating to 120 °C under helium gas flow.

Scheme 2. Hypothesized modulator/node dynamics

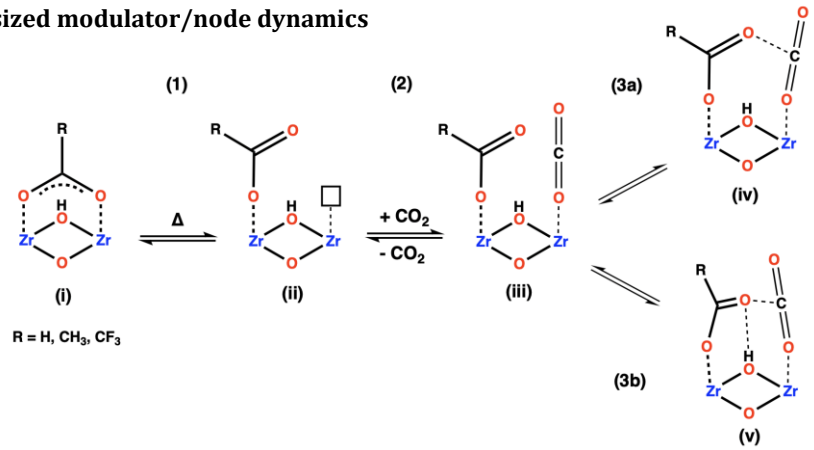

Based on these experimental observations, we propose a mechanistic pathway for CO_2 chemisorption to the zirconium node in Scheme 2 that is consistent with dependence on modulator identity and could lead to the observed spectroscopic behavior. In this pathway, both zirconium atoms of the node are initially capped by the two oxygens of the carboxylate modulator (i), after which dissociation of one oxygen (1) results in one capped and one uncapped metal site (ii). CO_2 can then directly access the open zirconium site (2) to fully cap the node (iii), after which the dangling electron-rich modulator oxygen either (3a) interacts directly with the electron-deficient carbon of CO_2 (iv) to form an eight-membered ring or (3b) the hydrogen of a μ^3-OH bridging group (v), to form two six-membered rings and stabilize the geometry about the node. This pathway is consistent with the modulator dependence of the 2335 cm^{-1} IR stretch, as well as its odd temperature-dependence and the absence of such behavior in MOFs with modulator removed. Additionally, the first step correlates with the observed experimental trends: the CF_3 group of trifluoroacetate withdraws electron density from the carboxylate oxygens and stabilizes a partially dissociated geometry, while the CH_3 group of acetate increases the electron density of these oxygens and destabilizes the same species.

In order to further investigate the viability of this explanation for the observed spectroscopic behavior, density functional theory (DFT) calculations were conducted on cluster models of the MOF-808 pore (See SI for details on selecting the representative cluster). The first adsorption mode tested was CO_2 physisorption on the zirconium node with the FA modulator bound through both carboxylate oxygens (configuration (i) in Scheme 2). The frequencies and enthalpies of adsorption for physisorption of CO_2 on different potential sites are reported in Figure 7 and Table 1. The frequencies of the CO_2 asymmetric stretching mode for the three physisorption sites ranged from 2338 to 2343 cm^{-1} (Table 1), in an excellent agreement with experimentally determined values. Adsorption on *Zr* and on μOH is more favorable than on μO, with the enthalpies of adsorption of approx. -24 kJ/mol and -12 kJ/mol, respectively, which follows the expected trend, where the adsorbate molecule interacts strongly with the hydroxyl group or a "pocket" created by the linker and two formate modulators.

Table 1. Frequencies of the CO_2 asymmetric stretching mode and enthalpies of adsorption for physisorption configurations on the MOF-808-FA node, tested in DFT c

Adsorption mode	Frequency of asymmetric stretching mode (cm^{-1})	ΔH_{ads} (kJ/mol)
Physisorption on *Zr*	2338	-24.3
Physisorption on μO	2343	-12.3
Physisorption on μOH	2340	-24.4

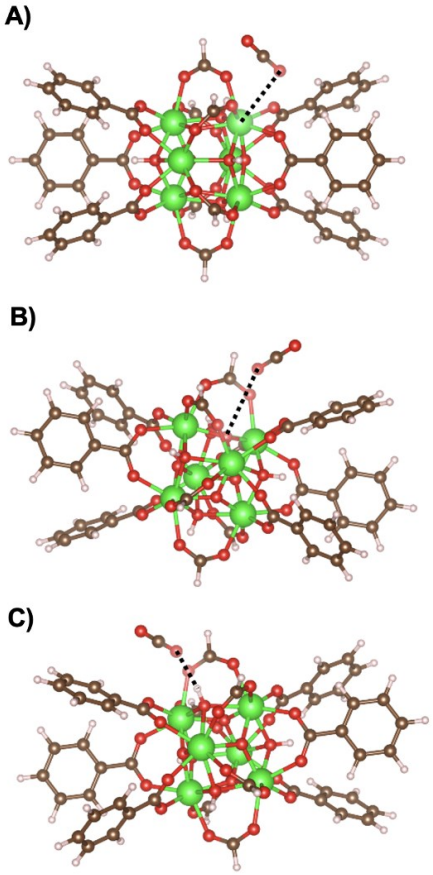

Figure 7. Three physisorption modes considered in DFT computations: CO_2 adsorbs on A) the Zr atom, B) the μO bridging atom or C) the μOH bridging atom of the MOF-808-FA node. Dotted lines added to clarify spatial configuration of the CO_2 molecule. (green = Zr, red = O, brown = C, white

To analyze the possibility of CO_2 chemisorption, we optimized structures in which one of the Zr-O bonds between the node and modulator was broken and oxygen from CO_2 coordinated to the open Zr site. The three generated configurations (Figure 8) differ in the position of the "dangling" carboxylate oxygen. The optimized Zr-O_{CO2} distances are 2.49 Å, 2.59 Å and 2.49 Å for configurations 8A, 8B and 8C, respectively which suggest strong interactions, as Zr-$O_{formate}$ bond lengths are approximately 2.25 Å. The corresponding observed frequencies range from 2337 to 2325 cm^{-1}, decreasing in frequency compared to physisorption as a consequence of the Zr ion pulling electron density from the bound O_{CO2}, which weakens the C-O bond in the guest molecule.

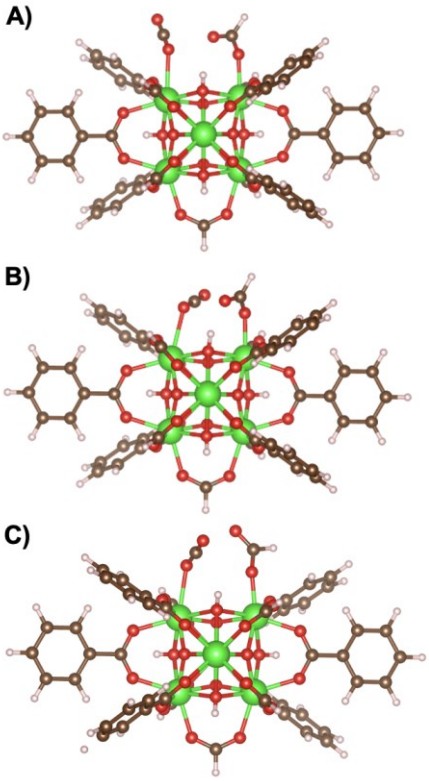

Figure calcula ylate o: move fi l in DFT carbox- owed to = H)

The stretching frequency of configuration 8B is approximately 2335 cm^{-1} which is in almost perfect agreement with experimental results, suggesting that this is the most plausible configuration for CO_2 chemisorption. While the calculated enthalpies of chemisorption are endothermic (Table 2), this could be a result of instability in the dangling oxygen from monodentate formate. A stabilizing factor not considered in these calculations likely exists that leads to stabilization beyond the binding of a single molecule, such as additional CO_2 molecules interacting with the node. While previous reports show that chemisorption can be exothermic in case of full modulator removal,[56] experimental results indicated that the number of modulators does not change before and after exposure to a CO_2 stream (Figures S1-S4).

Adsorption mode	Frequency of asymmetric stretching mode (cm^{-1})	ΔH_{ads} (kJ/mol)
Chemisorption on $Zr(\mu O)$ (8A)	2337	46.1
Chemisorption on $Zr(\mu OH)$ (8B)	2335	22.4
Chemisorption on Zr (8C)	2325	53.9

To further computationally probe the experimentally observed modulator effects on sorption, the monodentate formate modulator was replaced with acetate and trifluoroacetate. These calculations confirmed the experimental observation that the chemisorption is most likely to occur in the presence of TFA (Table 3), where $\Delta H_{chemisorption}$ decreases by 11 to 16 kJ/mol depending on configuration. Moreover, the decrease of the Zr-O bond strength (AA > FA > TFA) with changes in modulator agree with the decrease of natural bond orbital (NBO) charge on the oxygen atom of the modulator (-0.66, -0.64 and -0.61, respectively).

Table 3. Enthalpies of chemisorption of CO_2 in MOF-808 capped with different modulators.

Configuration	$\Delta H_{chemisorption}$ (kJ/mol)		
	MOF-808-FA	MOF-808-AA	MOF-808-TFA
8A	53.9	55.1	37.8
8B	22.4	22.5	11.2
8C	46.1	48.2	30.1

In combination with experimental findings, these calculations suggest that the pore structure within MOF-808, typically presumed to be static during gas sorption, is very dynamic. Not only does this represent a shift in perspective on potential surface engineering within MOF pores, it also suggests necessary improvements in computational adsorption studies, especially Monte Carlo simulations, where most previous reports consider the bonds of the capping modulator to the MOF node to be fully intact throughout sorption.

Conclusion

The structures of many metal-organic frameworks are very stable and thus often assumed to be static. Dynamic pore structures could lead to behavior otherwise inaccessible during gas sorption. The variety of modulators used to cap open metal sites of zirconium MOFs offers a promising handle to tune such dynamics. Spurred by the observation of unexpected *in situ* DRIFTS behavior during CO_2 sorption, we probed new possible chemisorption mechanisms. Our investigation indicated dynamic capping modulator behavior allowing CO_2 to directly chemisorb to open zirconium sites to various degrees depending on the identity of the modulator, specifically the electron density on the carboxylate oxygens. These dynamics and the cooperative interaction between the adsorbed CO_2 and hemilabile modulator represent new considerations when examining gas sorption mechanisms: modulator-node bonds in MOFs should not be considered static during gas sorption, and dynamic pore structures could be leveraged in the design of future sorbents.

ASSOCIATED CONTENT

Supporting Information

Full experimental details and additional figures (PDF); crystallographic files for the optimized cluster used in DFT calculations (CIF); node structures for nodes capped with FA (PDB), AA (PDB), or TFA (PDB); structures described for physisorption of CO_2 on Zr (PDB), O (PDB) or OH (PDB); structural representations of chemisorption described in figure 8A for nodes capped with FA (PDB), AA (PDB), and TFA (PDB); structural

representations of chemisorption described in figure 8B for nodes capped with FA (PDB), AA (PDB), and TFA (PDB); structural representations of chemisorption described in figure 8C for nodes capped with FA (PDB), AA (PDB), and TFA (PDB).

AUTHOR INFORMATION

Corresponding Author

***Omar K. Farha** – Department of Chemistry and International Institute for Nanotechnology, Northwestern University, Evanston, Illinois 60208, United States; orcid.org/0000-0002-9904-9845; Email: o-farha@u.northwestern.edu

Authors

Thomas M. Rayder – Department of Chemistry, Northwestern University, Evanston, Illinois 60208, United States; orcid.org/0000-0002-2488-1143; Email: rayder@northwestern.edu

Filip Formalik– Department of Chemical & Biological Engineering, Northwestern University, Evanston, IL 60208, United States; Department of Micro, Nano, and Bioprocess Engineering, Faculty of Chemistry, Wroclaw University of Science and Technology, 50-370 Wroclaw, Poland; orcid.org/0000-0003-3981-3298; Email: filip.formalik@northwestern.edu

Simon M. Vornholt – Department of Chemistry, Stony Brook University, Stony Brook, NY 11794, United States; orcid.org/0000-0001-9490-3785; Email: simon.vornholt@stonybrook.edu

Hilliary Frank – Department of Chemistry and Biochemistry, University of California, San Diego, La Jolla, CA 92037, United States; orcid.org/0000-0002-6363-5818; Email: hfrank@ucsd.edu

Seryeong Lee – Department of Chemistry, Northwestern University, Evanston, Illinois 60208, United States; Email: seryeonglee2026@u.northwestern.edu

Maytham Alzayer – Department of Chemical & Biological Engineering, Northwestern University, Evanston, Illinois 60208, United States; Email: maythamalzayer2023@u.northwestern.edu

Zhihengyu Chen – Department of Chemistry, Stony Brook University, Stony Brook, NY 11794, United States; orcid.org/0000-0001-5882-7076; Email: zhihengyu.chen@stonybrook.edu

Debabrata Sengupta – Department of Chemistry, Northwestern University, Evanston, Illinois 60208, United States; orcid.org/0000-0001-7212-3761; Email: debabrata.sengupta@northwestern.edu

Timur Islamoglu – Department of Chemistry, Northwestern University, Evanston, Illinois 60208, United States; orcid.org/0000-0003-3688-9158; Email: timur.islamoglu@northwestern.edu

Francesco Paesani – Department of Chemistry and Biochemistry, University of California, San Diego, La Jolla, CA 92037, United States; orcid.org/0000-0002-4451-1203; Email: fpaesani@ucsd.edu

Karena W. Chapman – Department of Chemistry, Stony Brook University, Stony Brook, NY 11794, United States; orcid.org/0000-0002-8725-5633; Email: karena.chapman@stonybrook.edu

Randall Q. Snurr – Department of Chemical & Biological Engineering, Northwestern University, Evanston, Illinois 60208, United States; orcid.org/0000-0003-2925-9246; Email: snurr@northwestern.edu

Author Contributions

The manuscript was written through contributions of all authors. All authors have given approval to the final version of the manuscript.

Notes

The authors declare the following competing financial interest(s): O.K.F. has a financial interest in the start-up company Nu-Mat Technologies, which is seeking to commercialize metal-organic frameworks.

Funding Sources

This work was funded by U.S. Department of Energy (DOE) grant DE-SC0022332 and the U.S. National Science Foundation (Award # 2119433).

ACKNOWLEDGMENT

This work is supported by U.S. Department of Energy (DOE) grant DE-SC0022332. F.F. is supported by the Polish National Agency for Academic Exchange (decision no. BPN/BEK/2021/1/00184/DEC). R.Q.S. acknowledges support from the U.S. National Science Foundation (Award #2119433). This research used resources of the National Energy Research Scientific Computing Center; a DOE Office of Science User Facility supported by the Office of Science of the U.S. Department of Energy under Contract No. DE-AC02-05CH11231 using NERSC award BES-ERCAP0023154. Gaussian calculations were done using resources provided by Wroclaw Centre for Networking and Supercomputing, grant No. 33. This research used beamline 11-ID-B of the Advanced Photon Source, a U.S. Department of Energy (DOE) Office of Science User Facility operated for the DOE Office of Science by Argonne National Laboratory under contract no. DE-AC02-06CH11357. *In situ* X-ray structural analyses and multivariate analysis of the DRIFTS data were supported by U.S. Department of Energy (DOE) grant DE-SC0022332. This work made use of the EPIC facility of Northwestern University's NUANCE Center, which has received support from the SHyNE Resource (NSF ECCS-2025633), the IIN, and Northwestern's MRSEC program (NSF DMR-1720139). T.M.R. wishes to acknowledge Zoha Syed and Selim Alayoglu for helpful discussions and assistance in initial experimental procedures.

REFERENCES

(1) Pachauri, R. K.; Allen, M. R.; Barros, V. R.; Broome, J.; Cramer, W.; Christ, R.; Church, J. A.; Clarke, L.; Dahe, Q.; Dasgupta, P.; Dubash, N. K.; Edenhofer, O.; Elgizouli, I.; Field, C. B.; Forster, P.; Friedlingstein, P.; Fuglestvedt, J.; Gomez-Echeverri, L.; Hallegatte, S.; Hegerl, G.; Howden, M.; Jiang, K.; Jimenez Cisneroz, B.; Kattsov, V.; Lee, H.; Mach, K. J.; Marotzke, J.; Mastrandrea, M. D.; Meyer, L.; Minx, J.; Mulugetta, Y.; O'Brien, K.; Oppenheimer, M.; Pereira, J. J.; Pichs-Madruga, R.; Plattner, G.-K.; Pörtner, H.-O.; Power, S. B.; Preston, B.; Ravindranath, N. H.; Reisinger, A.; Riahi, K.; Rusticucci, M.; Scholes, R.; Seyboth, K.; Sokona, Y.; Stavins, R.; Stocker, T. F.; Tschakert, P.; van Vuuren, D.; van Ypserle, J.-P. *Climate Change 2014: Synthesis Report. Contribution of Working Groups I, II and III to the Fifth Assessment Report of the Intergovernmental Panel on Climate Change*; Pachauri, R. K., Meyer, L., Eds.; IPCC: Geneva, Switzerland, 2014.

(2) Alivisatos, P.; Buchanan, M. Basic Research Needs for Carbon Capture: Beyond 2020; Nova Science Publishers, Inc.; 2010.

(3) National Academies of Sciences Engineering and Medicine. Negative Emissions Technologies and Reliable Sequestration: A Research Agenda; The National Academies Press: Washington, DC; 2019.

(4) Baciocchi, R.; Storti, G.; Mazzotti, M. Process Design and Energy Requirements for the Capture of Carbon Dioxide from Air. *Chemical Engineering and Processing: Process Intensification* **2006**, *45* (12), 1047–1058.
(5) Ozkan, M.; Custelcean, R.; Editors, G. The Status and Prospects of Materials for Carbon Capture Technologies. *MRS Bull* **2022**, *47* (4), 390–394.
(6) Kumar, S.; Srivastava, R.; Koh, J. Utilization of Zeolites as CO2 Capturing Agents: Advances and Future Perspectives. *Journal of CO2 Utilization* **2020**, *41*, 101251.
(7) Cherevotan, A.; Raj, J.; Peter, S. C. An Overview of Porous Silica Immobilized Amines for Direct Air CO2 Capture. *J Mater Chem A Mater* **2021**, *9* (48), 27271–27303.
(8) Pérez-Botella, E.; Valencia, S.; Rey, F. Zeolites in Adsorption Processes: State of the Art and Future Prospects. *Chem Rev* **2022**, *122* (24), 17647–17695.
(9) Nugent, P.; Belmabkhout, Y.; Burd, S. D.; Cairns, A. J.; Luebke, R.; Forrest, K.; Pham, T.; Ma, S.; Space, B.; Wojtas, L.; Eddaoudi, M.; Zaworotko, M. J. Porous Materials with Optimal Adsorption Thermodynamics and Kinetics for CO2 Separation. *Nature* **2013**, *495* (7439), 80–84.
(10) Ding, M.; Flaig, R. W.; Jiang, H.-L.; Yaghi, O. M. Carbon Capture and Conversion Using Metal–Organic Frameworks and MOF-Based Materials. *Chem Soc Rev* **2019**, *48* (10), 2783–2828.
(11) Custelcean, R. Direct Air Capture of CO2via Crystal Engineering. *Chem Sci* **2021**, *12* (38), 12518–12528.
(12) Howarth, A. J.; Liu, Y.; Li, P.; Li, Z.; Wang, T. C.; Hupp, J. T.; Farha, O. K. Chemical, Thermal and Mechanical Stabilities of Metal–Organic Frameworks. *Nat Rev Mater* **2016**, *1* (3), 15018.
(13) Furukawa, H.; Cordova, K. E.; O'Keeffe, M.; Yaghi, O. M. The Chemistry and Applications of Metal-Organic Frameworks. *Science (1979)* **2013**, *341* (6149), 1230444.
(14) Moghadam, P. Z.; Li, A.; Wiggin, S. B.; Tao, A.; Maloney, A. G. P.; Wood, P. A.; Ward, S. C.; Fairen-Jimenez, D. Development of a Cambridge Structural Database Subset: A Collection of Metal–Organic Frameworks for Past, Present, and Future. *Chemistry of Materials* **2017**, *29* (7), 2618–2625.
(15) Kumar, A.; Madden, D. G.; Lusi, M.; Chen, K.-J.; Daniels, E. A.; Curtin, T.; Perry IV, J. J.; Zaworotko, M. J. Direct Air Capture of CO2 by Physisorbent Materials. *Angewandte Chemie International Edition* **2015**, *54* (48), 14372–14377.
(16) Maia, R. A.; Louis, B.; Gao, W.; Wang, Q. CO2 Adsorption Mechanisms on MOFs: A Case Study of Open Metal Sites, Ultra-Microporosity and Flexible Framework. *React Chem Eng* **2021**, *6* (7), 1118–1133.
(17) Forse, A. C.; Milner, P. J.; Lee, J.-H.; Redfearn, H. N.; Oktawiec, J.; Siegelman, R. L.; Martell, J. D.; Dinakar, B.; Zasada, L. B.; Gonzalez, M. I.; Neaton, J. B.; Long, J. R.; Reimer, J. A. Elucidating CO2 Chemisorption in Diamine-Appended Metal–Organic Frameworks. *J Am Chem Soc* **2018**, *140* (51), 18016–18031.
(18) Flaig, R. W.; Osborn Popp, T. M.; Fracaroli, A. M.; Kapustin, E. A.; Kalmutzki, M. J.; Altamimi, R. M.; Fathieh, F.; Reimer, J. A.; Yaghi, O. M. The Chemistry of CO2 Capture in an Amine-Functionalized Metal–Organic Framework under Dry and Humid Conditions. *J Am Chem Soc* **2017**, *139* (35), 12125–12128.
(19) Cai, Z.; Bien, C. E.; Liu, Q.; Wade, C. R. Insights into CO2 Adsorption in M–OH Functionalized MOFs. *Chemistry of Materials* **2020**, *32* (10), 4257–4264.
(20) Bai, Y.; Dou, Y.; Xie, L.-H.; Rutledge, W.; Li, J.-R.; Zhou, H.-C. Zr-Based Metal–Organic Frameworks: Design, Synthesis, Structure, and Applications. *Chem Soc Rev* **2016**, *45* (8), 2327–2367.
(21) Ahmad, K.; Nazir, M. A.; Qureshi, A. K.; Hussain, E.; Najam, T.; Javed, M. S.; Shah, S. S. A.; Tufail, M. K.; Hussain, S.; Khan, N. A.; Shah, H.-R.; Ashfaq, M. Engineering of Zirconium Based Metal-Organic Frameworks (Zr-MOFs) as Efficient Adsorbents. *Materials Science and Engineering: B* **2020**, *262*, 114766.
(22) Yuan, S.; Qin, J.-S.; Lollar, C. T.; Zhou, H.-C. Stable Metal–Organic Frameworks with Group 4 Metals: Current Status and Trends. *ACS Cent Sci* **2018**, *4* (4), 440–450.
(23) Zhang, X.; Wang, B.; Alsalme, A.; Xiang, S.; Zhang, Z.; Chen, B. Design and Applications of Water-Stable Metal-Organic Frameworks: Status and Challenges. *Coord Chem Rev* **2020**, *423*, 213507.
(24) Lu, Z.; Liu, J.; Zhang, X.; Liao, Y.; Wang, R.; Zhang, K.; Lyu, J.; Farha, O. K.; Hupp, J. T. Node-Accessible Zirconium MOFs. *J Am Chem Soc* **2020**, *142* (50), 21110–21121.
(25) Mautschke, H.-H.; Drache, F.; Senkovska, I.; Kaskel, S.; Llabrés i Xamena, F. X. Catalytic Properties of Pristine and Defect-Engineered Zr-MOF-808 Metal Organic Frameworks. *Catal Sci Technol* **2018**, *8* (14), 3610–3616.
(26) Cirujano, F. G.; Llabrés i Xamena, F. X. Tuning the Catalytic Properties of UiO-66 Metal–Organic Frameworks: From Lewis to Defect-Induced Brønsted Acidity. *J Phys Chem Lett* **2020**, *11* (12), 4879–4890.
(27) Wang, H.; Dong, X.; Lin, J.; Teat, S. J.; Jensen, S.; Cure, J.; Alexandrov, E. v; Xia, Q.; Tan, K.; Wang, Q.; Olson, D. H.; Proserpio, D. M.; Chabal, Y. J.; Thonhauser, T.; Sun, J.; Han, Y.; Li, J. Topologically Guided Tuning of Zr-MOF Pore Structures for Highly Selective Separation of C6 Alkane Isomers. *Nat Commun* **2018**, *9* (1), 1745.
(28) Feng, L.; Day, G. S.; Wang, K.-Y.; Yuan, S.; Zhou, H.-C. Strategies for Pore Engineering in Zirconium Metal-Organic Frameworks. *Chem* **2020**, *6* (11), 2902–2923.
(29) Rayder, T. M.; Bensalah, A. T.; Li, B.; Byers, J. A.; Tsung, C.-K. Engineering Second Sphere Interactions in a Host-Guest Multicomponent Catalyst System for the Hydrogenation of Carbon Dioxide to Methanol. *J Am Chem Soc* **2021**, *143* (3), 1630–1640.
(30) Cohen, S. M. The Postsynthetic Renaissance in Porous Solids. *J Am Chem Soc* **2017**, *139* (8), 2855–2863.
(31) Kalaj, M.; Cohen, S. M. Postsynthetic Modification: An Enabling Technology for the Advancement of Metal–Organic Frameworks. *ACS Cent Sci* **2020**, *6* (7), 1046–1057.
(32) Li, H.; Wang, K.; Sun, Y.; Lollar, C. T.; Li, J.; Zhou, H.-C. Recent Advances in Gas Storage and Separation Using Metal–Organic Frameworks. *Materials Today* **2018**, *21* (2), 108–121.
(33) Cavka, J. H.; Jakobsen, S.; Olsbye, U.; Guillou, N.; Lamberti, C.; Bordiga, S.; Lillerud, K. P. A New Zirconium Inorganic Building Brick Forming Metal Organic Frameworks with Exceptional Stability. *J Am Chem Soc* **2008**, *130* (42), 13850–13851.
(34) Wang, T. C.; Vermeulen, N. A.; Kim, I. S.; Martinson, A. B. F.; Stoddart, J. F.; Hupp, J. T.; Farha, O. K. Scalable Synthesis and Post-Modification of a Mesoporous Metal-Organic Framework Called NU-1000. *Nat Protoc* **2016**, *11* (1), 149–162.
(35) Furukawa, H.; Gándara, F.; Zhang, Y.-B.; Jiang, J.; Queen, W. L.; Hudson, M. R.; Yaghi, O. M. Water Adsorption in Porous Metal–Organic Frameworks and Related Materials. *J Am Chem Soc* **2014**, *136* (11), 4369–4381.
(36) Rayder, T. M.; Adillon, E. H.; Byers, J. A.; Tsung, C.-K. A Bioinspired Multicomponent Catalytic System for Converting Carbon Dioxide into Methanol Autocatalytically. *Chem* **2020**, *6* (7), 1742–1754.
(37) Yuan, S.; Zou, L.; Li, H.; Chen, Y.-P.; Qin, J.; Zhang, Q.; Lu, W.; Hall, M. B.; Zhou, H.-C. Flexible Zirconium Metal-Organic Frameworks as Bioinspired Switchable Catalysts. *Angewandte Chemie* **2016**, *128* (36), 10934–10938.
(38) Marshall, R. J.; Forgan, R. S. Postsynthetic Modification of Zirconium Metal-Organic Frameworks. *Eur J Inorg Chem* **2016**, *2016* (27), 4310–4331.
(39) Li, Z.; Rayder, T. M.; Luo, L.; Byers, J. A.; Tsung, C.-K. Aperture-Opening Encapsulation of a Transition Metal Catalyst in a Metal-Organic Framework for CO <inf>2</Inf> Hydrogenation. *J Am Chem Soc* **2018**, *140* (26), 8082–8085.
(40) He, T.; Zhang, Y.-Z.; Kong, X.-J.; Yu, J.; Lv, X.-L.; Wu, Y.; Guo, Z.-J.; Li, J.-R. Zr(IV)-Based Metal-Organic Framework with T-Shaped Ligand: Unique Structure, High Stability, Selective Detection, and Rapid Adsorption of Cr2O72– in Water. *ACS Applied Materials & Interfaces* **2018**, *10* (19), 16650–16659.
(41) Chen, Y.; Zhang, X.; Ma, K.; Chen, Z.; Wang, X.; Knapp, J.; Alayoglu, S.; Wang, F.; Xia, Q.; Li, Z.; Islamoglu, T.; K. Farha, O.

Zirconium-Based Metal–Organic Framework with 9-Connected Nodes for Ammonia Capture. *ACS Appl Nano Mater* **2019**, *2* (10), 6098–6102.
(42) Liu, X.; Kirlikovali, K. O.; Chen, Z.; Ma, K.; Idrees, K. B.; Cao, R.; Zhang, X.; Islamoglu, T.; Liu, Y.; Farha, O. K. Small Molecules, Big Effects: Tuning Adsorption and Catalytic Properties of Metal–Organic Frameworks. *Chemistry of Materials* **2021**, *33* (4), 1444–1454.
(43) Lyu, H.; Chen, O. I.-F.; Hanikel, N.; Hossain, M. I.; Flaig, R. W.; Pei, X.; Amin, A.; Doherty, M. D.; Impastato, R. K.; Glover, T. G.; Moore, D. R.; Yaghi, O. M. Carbon Dioxide Capture Chemistry of Amino Acid Functionalized Metal–Organic Frameworks in Humid Flue Gas. *J Am Chem Soc* **2022**, *144* (5), 2387–2396.
(44) Park, J. M.; Yoo, D. K.; Jhung, S. H. Selective CO2 Adsorption over Functionalized Zr-Based Metal Organic Framework under Atmospheric or Lower Pressure: Contribution of Functional Groups to Adsorption. *Chemical Engineering Journal* **2020**, *402*, 126254.
(45) Thür, R.; van Havere, D.; van Velthoven, N.; Smolders, S.; Lamaire, A.; Wieme, J.; van Speybroeck, V.; de Vos, D.; Vankelecom, I. F. J. Correlating MOF-808 Parameters with Mixed-Matrix Membrane (MMM) CO2 Permeation for a More Rational MMM Development. *J. Mater. Chem. A* **2021**, *9* (21), 12782–12796.
(46) Andreeva, A. B.; Le, K. N.; Chen, L.; Kellman, M. E.; Hendon, C. H.; Brozek, C. K. Soft Mode Metal-Linker Dynamics in Carboxylate MOFs Evidenced by Variable-Temperature Infrared Spectroscopy. *J Am Chem Soc* **2020**, *142* (45), 19291–19299.
(47) Allendorf, M. D.; Stavila, V.; Witman, M.; Brozek, C. K.; Hendon, C. H. What Lies beneath a Metal–Organic Framework Crystal Structure? New Design Principles from Unexpected Behaviors. *J Am Chem Soc* **2021**, *143* (18), 6705–6723.
(48) Tan, K.; Pandey, H.; Wang, H.; Velasco, E.; Wang, K.-Y.; Zhou, H.-C.; Li, J.; Thonhauser, T. Defect Termination in the UiO-66 Family of Metal–Organic Frameworks: The Role of Water and Modulator. *J Am Chem Soc* **2021**, *143* (17), 6328–6332.
(49) According to Energy Dispersive X-Ray Spectroscopy (EDS) MOF-808-OH contained ~4.5 Cl- ions/node. Removal of these chloride ions by base treatment (see Ref. 50) did not change DRIFTS behavior, thus the node of MOF-808-OH in this work appears accurate.
(50) Lu, Z.; Liu, J.; Zhang, X.; Liao, Y.; Wang, R.; Zhang, K.; Lyu, J.; K. Farha, O.; T. Hupp, J. Node-Accessible Zirconium MOFs. *J Am Chem Soc* **2020**, *142* (50), 21110–21121.
(51) Experiments conducted with $^{13}CO_2$ confirmed that the observed IR stretches corresponded to gaseous CO_2 adsorbed on the MOF rather than atmospheric CO_2 or another MOF component (see SI for experimental details and Figure S25).
(52) O'Nolan, D.; Zhao, H.; Chen, Z.; Grenier, A.; Beauvais, M. L.; Newton, M. A.; Nenoff, T. M.; Chupas, P. J.; Chapman, K. W. A Multimodal Analytical Toolkit to Resolve Correlated Reaction Pathways: The Case of Nanoparticle Formation in Zeolites. *Chem Sci* **2021**, *12* (41), 13836–13847.
(53) Chen, Z.; Stroscio, G. D.; Liu, J.; Lu, Z.; Hupp, J. T.; Gagliardi, L.; Chapman, K. W. Node Distortion as a Tunable Mechanism for Negative Thermal Expansion in Metal–Organic Frameworks. *J Am Chem Soc* **2023**, *145* (1), 268–276.
(54) Hicks, K. E.; Wolek, A. T. Y.; Farha, O. K.; Notestein, J. M. The Dependence of Olefin Hydrogenation and Isomerization Rates on Zirconium Metal–Organic Framework Structure. *ACS Catal* **2022**, *12* (21), 13671–13680.
(55) Dehydrated MOF-808 (MOF-808-D) was prepared as described in previous reports (see Ref. 54 and SI) in order to provide a substrate whose nodes were fully accessible and uncapped by either modulator or aquo/hydroxyl Groups.
(56) Grissom, T. G.; Driscoll, D. M.; Troya, D.; Sapienza, N. S.; Usov, P. M.; Morris, A. J.; Morris, J. R. Molecular-Level Insight into CO2 Adsorption on the Zirconium-Based Metal–Organic Framework, UiO-66: A Combined Spectroscopic and Computational Approach. *The Journal of Physical Chemistry C* **2019**, *123* (22), 13731–13738.

Table of Contents Figure